Third European Conf. on Turbomachinery, IMech C557/074/99

Prediction of flow and heat transfer in a stationary two-dimensional rib roughened passage using low-Re turbulent models

J. BREDBERG and **L. DAVIDSON**
Department of Thermo and Fluid Dynamics, Chalmers University of Technology, Göteborg, Sweden

ABSTRACT

The flow field and heat transfer have been predicted with four different turbulence models, on two different rib-roughened channels. The turbulence models used were a zonal $k-\varepsilon$ model, two different $k-\omega$ models and an explicit algebraic Reynolds stress model (EARSM). The heat transfer model was a gradient Prandtl number model. The test cases included one low-Reynolds number, $Re = 12600$ and a high-Reynolds number, $Re = 122000$ rib-roughened 2D channel. The predicted flow field showed a good agreement with experimental results. The predicted heat transfer was, however, not as good and differed a lot between the turbulence models. No benefit was seen from using the more complex EARSM, but merely additional computational problems.

1 INTRODUCTION

Gas turbines which are operating at high gas temperature often need cooling of different structures in the engine. This project is focused on the internal cooling of the turbine blades. These blades generally have a rather complicated internal geometry. The cooling air enters through the root of the blade, and then flows along serpentine ducts and exits through either film-cooling holes or at the back of the blade. Inside the duct, transverse ribs are employed, which enhance the heat transfer. These ribs, which cause the flow to separate, raise the turbulence and heat transfer levels. Because the blades also rotate, these conditions add up to a very complicated environment for a turbulence modeler. In this study, as in numerous earlier studies, the geometry is simplified to a 2D duct, with square ribs normal to the flow direction. In addition only stationary cases are considered.

In this paper, the flow-field and heat transfer were predicted by the use of low-Reynolds number (LRN) turbulence models, which have previously been noted to be necessary in

these cases, [6]. The high-Reynolds number (HRN) turbulence models, which use wall functions have been shown not to capture the near-wall behavior accurately, which is necessary when predicting heat transfer. In the present study, three of the models are based on the eddy viscosity concept and one is an Explicit Algebraic Reynolds Stress Model (EARSM).

The main deficiency of the Eddy Viscosity Models (EVMs) is the isotropic description of the normal Reynolds stresses, which is a direct effect of the Boussinesq hypothesis. As a result of this deficiency results in that these models can not predict rotation and curvature effect, and do a fairly bad job when predicting accelerating flows. A physically more correct hypothesis, is to model the Reynolds stresses through their own transport equation, as in Reynolds Stress Models (RSM). These latter models enhance the quality of the predictions in more complicated environments, however at a considerably higher cost in CPU-time, combined with numerical stiffness and high complexity. The EARSM is seen as an intermediate step between the EVMs and the RSMs.

Most of the LRN EVMs used in the literature are based on the $k-\varepsilon$ model. A major deficiency of these models is the uncertainty of specifying the dissipation rate, ε at the walls.

The zonal or two-layer model of Chen and Patel [3] uses a composite approach to this problem. In this model, the eddy viscosity is calculated in the near-wall region with a one equation model of Wolfshtein [16], whereas in the outer region, it reverts to the standard $k-\varepsilon$ model.

Another way to circumvent the dissipation rate problem, is to discard the $k-\varepsilon$ concept altogether. This has been done successfully by Wilcox in recent years with the development of the $k-\omega$ model [13], [14]. A specially attractive feature of the LRN version of the $k-\omega$ model, is that the damping functions only depend on the turbulent Reynolds number, R_t. It is thus well suited for complex geometries where the wall distance may be difficult to obtain. In this paper two different $k-\omega$ models are used. The Peng *et al.* [10] $k-\omega$ model is based on the LRN version of Wilcox, [14], but adds a cross-diffusion term in the modeled ω equation. The second $k-\omega$ model is based on the standard version of Wilcox [13], see Abid *et al.* [2].

The EARSM is based on the assumptions made by Pope [11], where the Reynolds stresses are expressed explicitly. Pope's ideas were generalized to 3D by Gatski and Speziale [5]. The model used here is a 2D version of the EARSM by Gatski and Speziale with the Abid *et al.* $k-\omega$ model for the eddy viscosity description. The equation for the coefficient C_μ^* in the eddy viscosity concept used here is the modified version by Abid *et al.* [1]. This modification was made for numerical stability reasons.

In general, RSMs and EARSMs are known to be superior to EVMs in rotating flow, where the turbulence is highly non-isotropic. In this paper it will be investigated whether there are any benefits from using the more advanced turbulence models on a stationary 2D case, which might be viewed as case well suited for the eddy viscosity range of models.

2 FLOW EQUATIONS

2.1 Governing equations

The incompressible Reynolds averaged equations for mass, momentum and temperature are:

$$\frac{\partial U_i}{\partial x_i} = 0 \tag{1}$$

$$\rho\frac{DU_i}{Dt} = -\frac{\partial P}{\partial x_i} + \frac{\partial}{\partial x_j}\left(\mu\frac{\partial U_i}{\partial x_j} - \rho\overline{u_i u_j}\right) \tag{2}$$

$$\frac{DT}{Dt} = \frac{\partial}{\partial x_i}\left[\frac{\mu}{Pr}\frac{\partial T}{\partial x_i} - \rho\overline{u_i t}\right] \tag{3}$$

where $D/Dt = \partial/\partial t + U_j\partial/\partial x_j$. In the momentum and temperature equations several unknowns appear, due to the Reynolds-averaging procedure. These are the Reynolds stresses, $\overline{u_i u_j}$ and the turbulent heat fluxes, $\overline{u_i t}$, which will be modeled in the next sections.

2.2 Eddy viscosity based turbulent models

In the eddy viscosity models the Reynolds stresses are modeled by the Boussinesq hypothesis, which connects the unknown stresses with an apparent eddy viscosity, ν_t:

$$\overline{u_i u_j} = \frac{2}{3}k\delta_{ij} - 2\nu_t S_{ij} \tag{4}$$

where $S_{ij} = 0.5(\partial U_i/\partial x_j + \partial U_j/\partial x_i)$. In the most commonly used EVMs, the eddy viscosity is based on two turbulence properties, the turbulent kinetic energy k and a turbulent length scale l or its equivalent, such as the dissipation rate, ε, or the specific dissipation, ω. In this paper three turbulent models based on the eddy viscosity concept are used: the $k-\omega$ model of Peng *et al.* (PDH) [10]; the $k-\omega$ of Abid *et al.* (ARG) [2], and the two-layer $k-\varepsilon$ model of Chen and Patel (Zonal) [3].

Zonal $k-\varepsilon$ model The two-layer, or zonal, $k-\varepsilon$ model [3] uses two different approaches to compute the eddy viscosity: one in the main flow, or high-Reynolds number flow, and another in the near wall region, or the low-Reynolds number flow. The matching line between the two regions is set at $y^+ \approx 50$, where $y^+ = yu_\tau/\nu$. The HRN model is the standard $k-\varepsilon$ model, whereas the LRN model is the one-equation model by Wolfshtein [16]. The latter, as opposed to LRN $k-\varepsilon$ models, only requires the solution of one transport equation, that governing the turbulent kinetic energy. In this model the dissipation rate is set with the aid of a prescribed turbulence length scale. This concept removes the problematic boundary condition for the dissipation rate, with the turbulence length scale being a simple function of the wall distance.

ARG $k-\omega$ model The Abid *et al.* model [2] is based on the standard Wilcox $k-\omega$ model [13], however with a reformulation of the specific dissipation. Instead of using the Wilcox definition: $\omega = \varepsilon/(\beta^* k)$, $\beta^* = 0.09$, a true specific dissipation was used: $\omega \equiv \varepsilon/k$. With this change, C_μ is given the well-accepted value of 0.09 in the log-layer.

PDH $k-\omega$ model The $k-\omega$ model by Peng *et al.* [10] is similar to the LRN of Wilcox [14], however with a cross-diffusion term added in the ω equation. Furthermore, the coefficients and the wall-damping functions are re-tuned.

2.3 Explicit Algebraic Reynolds Stress Model (EARSM)

The basis for the EARSM is the transport equation for the Reynolds stresses. Following the same ideas as Rodi, the transport of Reynolds stresses is set equal to the normalized transport of kinetic energy. Adding a linear relation for the pressure-strain term, a explicit relation for the Reynolds stresses is given as:

$$\begin{aligned} \overline{u_i u_j} &= \frac{2}{3}k\delta_{ij} \\ -2\nu_t^* \left[\left(S_{ij} - \frac{1}{3}S_{kk}\delta_{ij} \right) + \frac{\alpha_4}{\omega}\left(S_{ik}\Omega_{kj} + S_{jk}\Omega_{ki} \right) - \frac{\alpha_5}{\omega}\left(S_{ik}S_{kj} - \frac{1}{3}S_{kl}S_{kl}\delta_{ij} \right) \right] \end{aligned} \tag{5}$$

where $\Omega_{ij} = 0.5(\partial U_i/\partial x_j - \partial U_j/\partial x_i)$. In the model by Abid *et al.* [2] this relation is used together with an $k-\omega$ EVM, where the eddy viscosity is defined as:

$$\nu_t^* = C_\mu^* \frac{k}{\omega} \tag{6}$$

and C_μ^* depends on the flow:

$$\begin{aligned} C_\mu^* &= \alpha_1 \frac{3\left(1+\eta^2\right) + 0.2\left(\eta^6 + \xi^6\right)}{3 + \eta^2 + 6\eta^2\xi^2 + 6\xi^2 + \eta^6 + \xi^6} \\ \eta^2 &= \frac{\alpha_2 S_{ij} S_{ij}}{\omega^2}, \qquad \xi^2 = \frac{\alpha_3 \Omega_{ij}\Omega_{ij}}{\omega^2} \end{aligned} \tag{7}$$

Note that the expression for C_μ^* has been changed to agree with Abid *et al.* [1] for numerical stability reasons. The constants ($\alpha_1, \alpha_2, \alpha_3, \alpha_4$ and α_5) depend on the pressure-strain model, which in this study was chosen to be the LRR model by Launder *et al.*, [7]. In the expression for the eddy viscosity Eq. (6), two additional transport equations are needed. In this paper, the Abid *et al.* model [2] was employed. However, virtually any EVM could be used, with a proper re-tuning of the constants and any damping functions.

2.4 Heat Transfer Model

In this paper the turbulent heat fluxes, $\overline{u_i t}$ are modeled with a simple gradient relation using a turbulent Prandtl number:

$$-\overline{u_i t} = \frac{\nu_t}{Pr_t}\frac{\partial T}{\partial x_i} \tag{8}$$

This model is used for both the EVMs and the EARSM, even though the EARSM predicts the Reynolds stresses and thus a more elaborated model could be feasible, such as the generalized gradient diffusion hypothesis (GGDH). From previous research in these flow conditions, any advantages of the GGDH over the turbulent Prandtl number have been slight according to Raisee, [12], and therefore the GGDH was not considered here. A turbulent Prandtl number of $Pr_t = 0.92$ was chosen, which is common for near-wall air flows.

3 NUMERICAL ASPECTS

3.1 Solver

A finite volume solver, CALC-BFC [4], was employed, which solves the flow equations in a fixed Cartesian co-ordinate system. The code uses a non-orthogonally co-located grid, with boundary fitted coordinates. SIMPLEC is used for the pressure-velocity coupling.

3.2 Periodic flow implementations

The cases examined here have a geometrical pattern which repeats itself after a certain distance in the stream-wise direction, i.e. the flow is periodic. These geometrical modules have identical inlet and outlet flow data, except for the pressure and temperature field. This makes it suitable, after modifications, to perform the calculations for only one of these modules, with a correspondingly reduced computational effort. The governing equations, Eqs. (1), (2) and (3), however need to be modified. The reason for this is that pressure and temperature do not repeat themselves in each module, since they continuously decay/increase along the stream-wise direction. In a periodic flow regime the pressure P and temperature T can be decomposed into a fluctuating term and a linear varying term in the stream-wise direction [9]. In a 2D case with periodic condition in the x-direction the following apply:

$$\begin{aligned} T(x,y) &= \tilde{T}(x,y) + \frac{d\overline{T}}{dx}x \\ P(x,y) &= \tilde{P}(x,y) - \frac{d\overline{P}}{dx}x \end{aligned} \tag{9}$$

where the fluctuating terms, $\tilde{P}(x,y)$ and $\tilde{T}(x,y)$, identically repeat themselves in each module. The linear temperature increase is given by the heat flux and mass flow:

$$\frac{d\overline{T}}{dx} = \frac{\dot{Q}}{\dot{m}c_p L} \tag{10}$$

The level of the pressure gradient has to be found iteratively. Substitution of the above fluctuating pressure $\tilde{P}$ and temperature $\tilde{T}$, adds source terms in the momentum equation ($d\overline{P}/dx\delta_{i1}$) and in the temperature equation ($-\rho U_i d\overline{T}/dx\delta_{i1}$), both of which will appear on the right-hand sides of Eq. (2) and Eq. (3) respectively.

3.3 Boundary conditions

As discussed above, periodic boundaries were enforced at the inlet and outlet. The walls were set as no-slip conditions. Uniform heat flux on the lower wall and adiabatic boundary condition on the upper wall were applied. The heat flux on the three rib faces, denoted AB, BC and CD in Fig. 1, was set to 1/3 of the nominal heat flux, to yield a constant total heat flux through the base area of the lower wall. This simplified heat flux wall condition may result in some discrepancies in the predicted Nusselt number (see later discussion).

Due to the fact that ω in the $k-\omega$ model is indefinite at the walls the near wall cells were set as:

$$\omega = \text{constant}\frac{\nu}{C_{\omega 2}y^2} \tag{11}$$

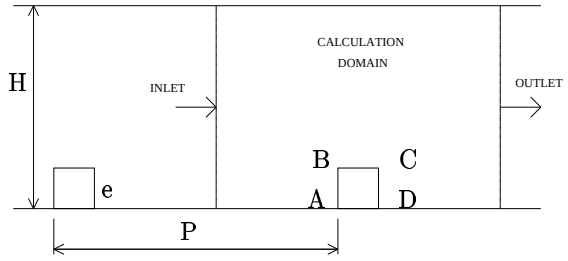

Re	122000	37200	12600
Pr	0.72	0.72	0.72
P/e	10	7.2	7.2
H/e	10	5	5
Exp. Data	[6]	[8]	[8]

Figure 1: **Data for the testcases**

which is valid for $y^+ < 2.5$, [15]. According to Wilcox, seven to ten nodes should be within this range, which could not be fulfilled in the present predictions, especially for the higher Reynolds number cases. For the two-layer $k-\varepsilon$ model, the partition line between the HRN model and LRN model was pre-selected to coincide with certain grid-lines. The results for the nodes with $y^+ \leq 50$ were therefore obtained with the LRN model.

4 RESULTS

Two different rib-roughened channels were used to evaluate the turbulence models. The configurations are depicted in Fig. 1. Data for the three different cases are also shown in Fig. 1, where P, H and e are as indicated. The Reynolds number is based on either the channel height ($Re = 122000$ case) or the hydraulic diameter (the other cases) and the bulk velocity. Experimental data are only given for the flow-field in the $Re = 37200$ case, and only for the Nusselt number in the other two cases.

The $Re = 37200$ and $Re = 12600$ cases were computed on the same mesh, $ni \times nj = 80 \times 120$, whereas the $Re = 122000$ case uses a $ni \times nj = 110 \times 120$ mesh. A grid-independence check is shown, for both the $Re = 12600$ and the $Re = 122000$ testcase, in Fig. 2. The coarse meshes measured 80×70 ($Re = 12600$ case) and 60×60 ($Re = 122000$ case) while the fine meshes measured 160×160 and 140×180 respectively. The predicted Nusselt number with the PDH $k-\omega$ model is almost indistinguishable between the fine and the medium grid. The coarse grid results differs by about 10 percent from the other two. The medium mesh was considered as good enough and used in the following predictions. Note that the abscissa in the $Re = 12600$ case is defined along the actual surface on the lower wall, that is, it follows the rib surface, and includes the surface denoted ABCD in Fig. 1. Each of these corners are indicated in Fig. 2(b) with a line, starting from left to right, as corners A, B, C and D. This explains the coordinate range in Fig. 2(b), which normalized with H should be from $x/H = 0$ to $x/H = 1.44$. However, including the faces AB and CD adds $0.2 + 0.2$ for a total of 1.84.

The rather big difference between the coarse mesh and the other two, is a result of the wall condition for the specific dissipation. For the three different meshes, the specific dissipation rate was fixed, using Eq. 11, for the first (coarse mesh), the first two (medium mesh) and first three nodes (fine mesh), respectively. This is in accordance with Wilcox [15] who uses the relation in Eq. 11 up to $y^+ = 2.5$. In the present computations however, only nodes which were within $y^+ \approx 1$ were fixed. It seems unlikely that fixing the specific dissipation for up to seven or even ten nodes, as suggested by Wilcox, is required. It can be noted that for the medium mesh, 5 nodes, 3 nodes and 2 nodes, respectively were within $y^+ = 2.5$ for the three test cases, $Re = 12600$, $Re = 37200$, and $Re = 122000$. Furthermore, the first two nodes were within $y^+ < 1$ for the lower Reynolds number case,

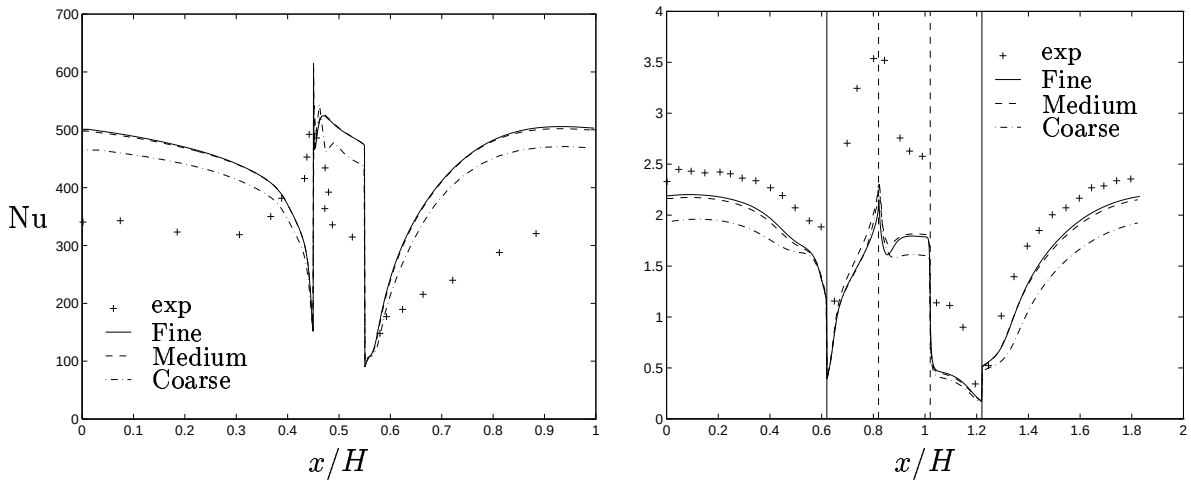

(a) $Re = 122000$ (b) $Re = 12600$

Figure 2: **Grid independence test, PDH $k-\omega$ model** [10]

and at least one node with $y^+ < 1$ for the higher Reynolds number cases. When using the zonal $k-\varepsilon$ model, between 25 and 10 nodes were calculated with the one-equation model, slightly fewer nodes for the higher Reynolds number cases.

The stream-wise velocity profiles for the $Re = 37200$ case at different locations are plotted in Fig. 3. The results are very similar for all models and they agree well with the experimental data, apart from the near wall region on the rib top, see Figs 3(a) and 3(b). This indicates that the recirculation bubble on the rib top may not be accurately captured. The most notable difference between the models is that the EARSM gives a rather large recirculation region downstream of the rib, in contradiction with the experiment, see Fig. 3(d).

Heat transfer predictions are usually visualized in terms of the Nusselt number. In the case of a prescribed heat transfer at the wall, q_w, it is defined as:

$$Nu = \frac{2q_w PrH}{\mu c_p(T_w - T_{bulk})} \tag{12}$$

where H is the channel height, Pr the Prandtl number, ν the viscosity, T_w the wall temperature and T_{bulk} the bulk temperature.

Predicted and experimental Nusselt numbers along the lower wall for the $Re = 122000$ case are shown in Fig. 4(a). The general trend is captured with all models, with the zonal model performing best. However, the values predicted with the $k-\omega$ based models are too high, whereas for the zonal model they are too low. This high Reynold number test case proved to be a difficult test. The heavily stretch grid, enforced by the low y^+ condition at the wall, may be the reason for poor convergence and bad results.

For the $Re = 12600$ case, the Nusselt number is normalized with the empirical Dittus-Boelter formula:

$$Nu_s = 0.023 \cdot Re^{0.8} \cdot Pr^{0.4} \tag{13}$$

The result for the $Re = 12600$ case is shown in Fig. 4(b).

Except for the rib top, the results for the PDH $k-\omega$ are rather good. The reason for the low Nusselt number on the rib, for all predictions, may be a result of both the

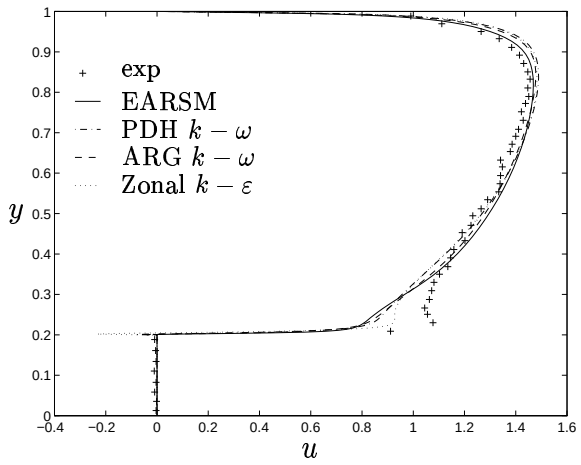

(a) **Velocity profiles at x/e = 0.1**

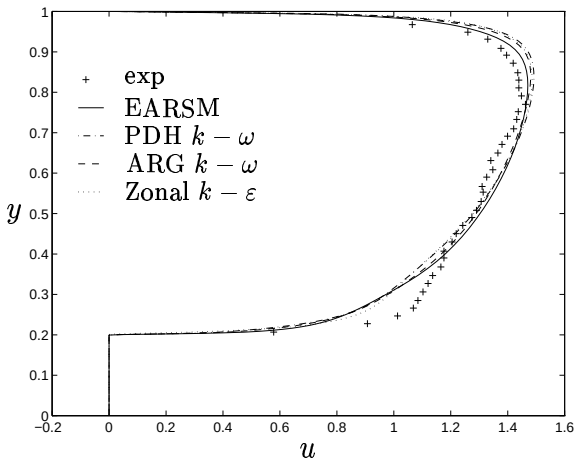

(b) **Velocity profiles at x/e = 0.5**

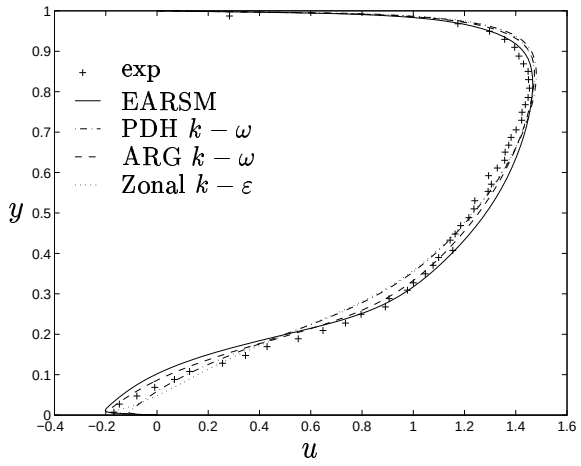

(c) **Velocity profiles at x/e = 4.18**

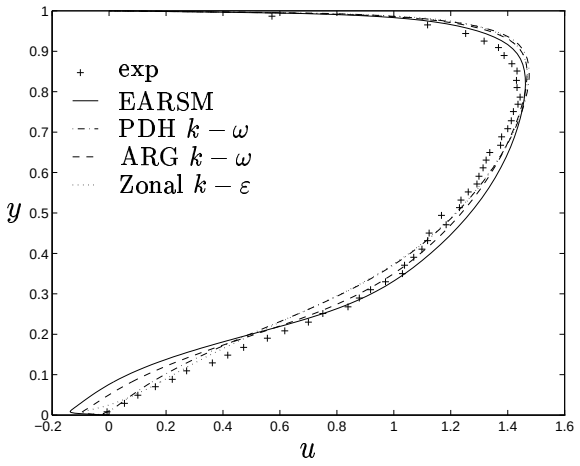

(d) **Velocity profiles at x/e = 5.32**

Figure 3: **Velocity profiles at various locations, Re = 37200. x is measured from the upstream corner (B in Fig. 1)**

prescribed heat flux and the discrepancy in the velocity profiles here. The experiment probably applied a constant heat flux through the lower wall, with conduction taking care of the distribution of the heat flux through the rib. However, due to lack of detailed information regarding the experiment, a simple constant heat flux wall condition was used in the computations. The predicted velocity profiles on the rib top indicate a too low level of turbulent energy close to the wall. This would then decrease the predicted Nusselt number through the heat transfer model, see Eq. 8. The ARG $k-\omega$ and the EARSM give similar results, with an overall lower predicted Nusselt number than the PDH $k-\omega$. This is most likely a consequence of the lower near wall turbulence levels predicted with the ARG $k-\omega$, which is a well known difference between a high Reynolds $k-\omega$ (ARG) and a low Reynolds $k-\omega$ (PDH). The main effect of the EARSM seems to be its more gradual rise after the rib. The zonal model gives a similar trend as for the $Re = 122000$ case, with an overall too low value.

Note also the difference in the experimental results up-stream of the rib, which gives

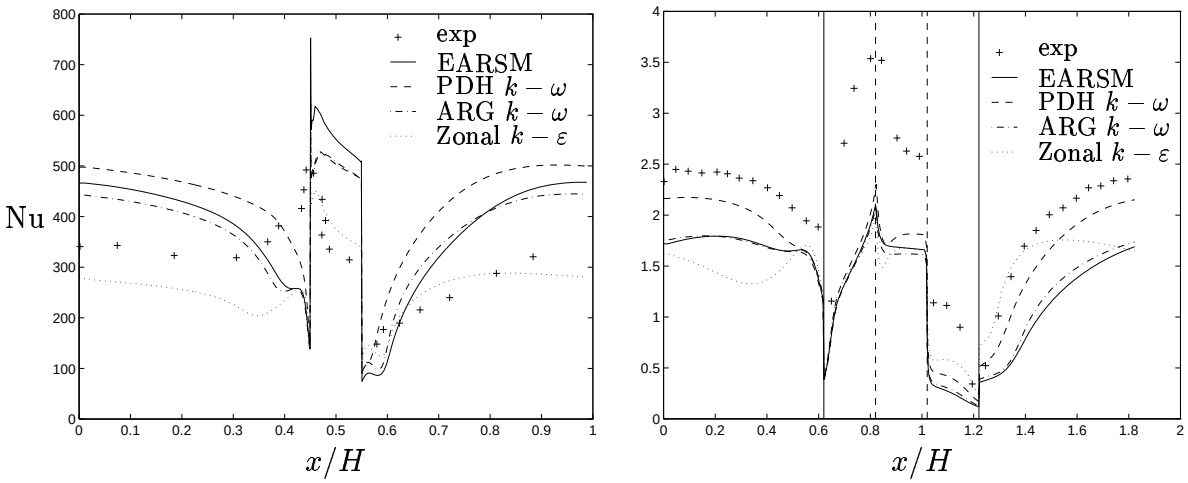

(a) $Re = 122000$ (b) $Re = 12600$

Figure 4: **Nusselt number for the two testcases**

an increase in Nusselt number for the HRN case, but a decrease for the LRN case. This is most probably not a direct result of the Reynolds number but due to the changes in the geometry. In the LRN case, the flow barely re-attaches before its separate again, whereas for the HRN case enough space is available for re-attachment and then separation to form a more rigid bubble in front of the rib.

5 CONCLUSIONS

The results for the flow field are in good agreement with the experiments apart from on the rib top, with slight differences between the various models. The only notable differences occur at the most downstream location, Fig. 3(d), where the EARSM predicts a too large re-circulation region.

The heat transfer results were generally much worse, and a more advanced heat transfer model and/or turbulence model is probably needed. The PDH $k-\omega$ model, which gave the best results for the $Re = 12600$ test case, gave the worst for the $Re = 122000$ test case. The zonal $k-\varepsilon$ shows the same trend for both Reynolds numbers, but predicts too low heat transfer in both cases. A notable problem for the zonal model was the matching line between the LRN and HRN model. This should occur at $y^+ \approx 50$, however, around the rib this could not be fulfilled due to conflicting constraints. A node could be close to the rib wall but far away from the channel wall, which made the prescribed partition between the HRN and LRN model somewhat difficult. Unfortunately the location of the dividing line also had an impact on the heat transfer results, and thus a model based on wall distances is not really suitable for these geometries. The ARG $k-\omega$ generated similar results as the PDH $k-\omega$ model with overall lower Nusselt number. The EARSM predictions did not differ much from the ARG $k-\omega$ model.

References

[1] R. Abid, J.H. Morrison, T.B. Gatski, and C.G. Speziale. Prediction of aerodynamic flows with a new explicit algebraic stress model. *AIAA Journal*, 34:2632–2635, 1996.

[2] R. Abid, C. Rumsey, and T. Gatski. Prediction of nonequilibrium turbulent flows with explicit algebraic stress models. *AIAA Journal*, 33:2026–2031, 1995.

[3] H.C. Chen and V.C. Patel. Near-wall turbulence models for complex flows including separation. *AIAA Journal*, 26:641–649, 1988.

[4] L. Davidson and B. Farhanieh. CALC-BFC. Report 95/11, Department of Thermo and Fluid Dynamics, Chalmers University of Technology, Gothenburg, 1995.

[5] T.B. Gatski and C.G. Speziale. On explicit algebraic stress models for complex turbulent flows. *J. Fluid Mechanics*, 254:59–78, 1993.

[6] H. Iacovides and M. Raisee. Computation of flow and heat transfer in 2-D rib roughened passages. In K. Hanjalić and T.W.J. Peeters, editors, *2nd Int. Symp. on Turbulence Heat and Mass Transfer (Addendum)*, pages 21–30, Delft, 1997. Delft University Press.

[7] B.E. Launder, G.J. Reece, and W. Rodi. Progress in the development of a Reynolds-stress turbulence closure. *J. Fluid Mechanics*, 68:537–566, 1975.

[8] T-M. Liou, J-J. Hwang, and S-H. Chen. Simulation and measurement of enhanced turbulent heat transfer in a channel with periodic ribs on one principal wall. *Int. J. Heat and Mass Transfer*, 36:507–517, 1993.

[9] S.V. Patankar, C.H. Liu, and E.M. Sparrow. Fully developed flow and heat transfer in ducts having streamwise-periodic variations of cross-sectional area. *J. Heat Transfer*, 99:180–186, 1977.

[10] S-H. Peng, L. Davidson, and S. Holmberg. A modified low-Reynolds-number $k-\omega$ model for recirculating flows. *J. Fluid Engineering*, 119:867–875, 1997.

[11] S.B. Pope. A more general effective-viscosity hypothesis. *J. Fluid Mechanics*, 72:331–340, 1975.

[12] M. Raisee. Heat transfer models in rib roughened passages. Private communication Dept. of Mechanical Engineering, UMIST, 1998.

[13] D.C. Wilcox. Reassessment of the scale-determining equation for advanced turbulence models. *AIAA Journal*, 26:1299–1310, 1988.

[14] D.C. Wilcox. Comparison of two-equation turbulence models for boundary layers with pressure gradient. *AIAA Journal*, 31:1414–1421, 1993.

[15] D.C. Wilcox. *Turbulence Modeling for CFD*. DCW Industries, Inc., 1993.

[16] M. Wolfshtein. The velocity and temperature distribution in one-dimensional flow with turbulence augumentation and pressure gradient. *Int. J. Heat and Mass Transfer*, 12:301–318, 1969.